Elson DS, Li R, Dunsby C, Eckersley R, Tang M-X Ultrasound-mediated optical tomography: a review of current methods INTERFACE FOCUS **1**(4):632-648 06 Aug 2011

Ultrasound-mediated optical tomography – a review of current methods

Daniel S. Elson[1], Rui Li[2], Christopher Dunsby[3], Robert Eckersley[4], and Meng-Xing Tang[2]

[1]Hamlyn Centre for Robotic Surgery, Department of Surgery and Cancer, Imperial College London, Exhibition Road, London SW7 2AZ, UK;
[2]Department of Bioengineering, Imperial College London, Exhibition Road, London, SW7 2AZ;
[3]Department of Physics, Imperial College London, Exhibition Road, London, SW7 2AZ;
[4]Imaging Sciences Department, Imperial College London, Du Cane Road, London W12 0HS

Summary

Ultrasound-mediated optical tomography (UOT) is a hybrid technique that is able to combine the high penetration depth and high spatial resolution of ultrasound imaging to overcome the limits imposed by optical scattering for deep tissue optical sensing and imaging. It has been proposed as a method to detect blood concentrations, oxygenation and metabolism at depth in tissue for the detection of vascularised tumours or the presence of absorbing or scattering contrast agents. In this paper the basic principles of the method are outlined and methods for simulating the UOT signal are described. The main detection methods are then summarised with a discussion of the advantages and disadvantages of each. The recent focus on increasing the weak UOT signal through the use of the acoustic radiation force is explained, together with a summary of our results showing sensitivity to the mechanical shear stiffness and optical absorption properties of tissue mimicking phantoms.

Key index words or phrases

Acousto-optics, ultrasound-mediated optical tomography (UOT), acoustic radiation force (ARF)

Introduction

Optical imaging of tissue has great diagnostic promise due to the strong and complex interaction of light with the different components of tissue, which has been shown to reveal rich physiological information. Besides the diversity of interaction methods and information available, light has the additional advantages of being non-ionising and generally non-harmful within published average and peak intensity limits [1], and the possibility of applications across length scales from microscopic (micron or sub-cellular resolution) to macroscopic (10's centimetre field of views). The main limiting factors that determine the design and performance of many tissue optical imaging systems are the strong absorption and scattering of light that occurs in tissues. This limits the penetration depth of some optical imaging modalities to the superficial tissue layers up to a few millimetres. For instance, white light illumination, or narrow band reflection or fluorescence imaging endoscopes can image the surface layers of tissues either in a large field of view endoscope [2,3,4] or with microscopic resolution [5, 6] at a few hundred microns imaging depth. To go beyond this depth and up to one or two millimetres, more sophisticated methods must be used such as two photon excited fluorescence, which uses the higher penetration depth of infrared light [7], or coherent techniques such as optical coherence tomography which detects only ballistic (reflected, back-scattered) photons using interferometry and rejects other scattered light [8].

For deeper tissue imaging, light that is in the 'tissue optical transmission window' (650 – 900 nm [9]) must be used, where absorption due to haemoglobin is minimised and absorption due to water is still relatively low. In general it is not possible to detect ballistic photons and the spatial resolution is degraded to ~10 mm by using techniques such as diffuse optical tomography (DOT) due to the many scattering events that occur as the light propagates through the tissue. The optical properties also limit the tissues that may be imaged to those that are relatively homogenous and/or low absorbing such as breast and brain [10]. In DOT, the output light distribution for a number of different light inputs is recorded, which subsequently allows the distribution of scatterers and absorbers to be calculated, usually only with a ~10 millimetre resolution at a few centimetre imaging depth due to the ill-posed nature of the inverse problem [11]. It is normally assumed that the absorption mainly comes from oxy- and deoxy-haemoglobin, which have slightly different absorption spectra [9] and may be used to obtain vascular and metabolic information about the tissue – important indicators of tumour development. A number of approximations may be made about the scattering properties of the tissue, so that the diffusion equation can be applied [10]. This has led to potential applications for DOT in detection of breast cancer, where higher concentrations of haemoglobin are used to identify cancerous lesions, and in neonatal brain imaging where the developmental response may be continuously and non-invasively monitored [10].

The aim of ultrasound-mediated optical tomography (UOT/UMT, often also referred to as ultrasound modulated optical tomography, ultrasound-assisted optical tomography (UAOT), acousto-photonic imaging (API) or acousto-optic imaging (AOI)) is to achieve high spatial resolution sensitive to optical absorption by creating an artificial marker or beacon at some depth in the tissue. This beacon is created throughout the volume of the beam with highest spatial resolution and sensitivity at the ultrasound focal region. This ultrasound beam modulates the local refractive index and optical scatterer positions, which in turn modulates the phase of photons that pass through this region (sometimes these photons are referred to as 'tagged photons' in the literature [12]). These photons are highly scattered as they travel from the ultrasound volume to the boundary of the tissue, but the relative number of photons that passed through the ultrasound beam may still be approximated by recording the intensity of the signal that exits the tissue surface that is modulated at the acoustic frequency. If the ultrasound focus is in an optical absorbing region then the modulation depth of the output signal is decreased because the acoustically modulated photons are absorbed. There is therefore the possibility of measuring the optical absorption properties of the tissue within a volume determined by the resolution properties of the acoustic beam. It is also possible to determine the scattering properties, for example by performing UOT at different ultrasound pressures [13].

It is thus said that UOT has the possibility of combining the advantages of optical imaging through the strong functional potential of haemoglobin (or an extrinsic contrast agent) imaging, and the advantages of ultrasound through the high tissue penetration depth, good spatial resolution and low scattering. The potential application areas of the technique overlap with those for DOT, for instance for breast cancer imaging, where the current modalities of mammography and ultrasound are not sufficient due to the use of ionising radiation and/or the lack of contrast or signal specificity between the healthy and disease tissues [14]. Besides bulk tissue tomography there are also other niche applications in subsurface detection of tumours, for instance in the neck [14], or for brain imaging [15, 16] to monitor the local oxygenation level and to allow the imaging of brain tumours and injuries. Further applications have been suggested, for instance in the assessment of osteoporosis [17], and more recently high resolution UOT has been used for detecting sentinel lymph nodes that have been labelled with an exogenous optical absorber [18]. It has also been shown that UOT could be used to

monitor therapy using high-intensity focused ultrasound using the same ultrasound geometry both for the lesion formation and detection [19]. Recent reviews of the use of UOT may be found in the following [20,21,22,23].

The main challenge for UOT is to efficiently detect the small modulated signal from the photons that passed through the ultrasound focus on top of the large background of unmodulated light. It is inconvenient that the signal is spread across a large area of the tissue surface and is travelling in all directions due to the high degree of optical scattering, leading to the requirement for large etendue (the product of the emitting surface and the solid angle) detectors. In addition, the random paths followed by photons reaching the detector result in random pathlength differences, causing an interference speckle pattern consisting of a distribution of bright and dark spots (a speckle pattern) [24]. The phase of the time-varying intensity modulation of these spots with respect to the ultrasound phase is random, and therefore simple spatial averaging of the speckle pattern by a single photodetector cannot directly increase the strength of the modulated optical signal. Furthermore, the random motions of the scatterers in the sample, for instance the movement of blood, decorrelates the speckle pattern and places a limit on the speed at which the signal must be collected. These effects will be described in more detail later in this paper.

UOT can be contrasted with photo acoustic imaging (PAT) (also called opto acoustic imaging) an alternative method using light and ultrasound that also combines the advantages of good ultrasound resolution with optical specificity. In this technique short (nanosecond) pulses of light illuminate a tissue causing a local thermoelastic expansion which results in an acoustic wave. The distribution of optical absorbers in the tissue can be calculated by recording the temporal and spatial evolution of the ultrasound trace. Note that the resolution in PAT comes primarily from optical absorption contrast, whereas UOT may also be sensitive to changes in optical scattering [25]. For further information refer to recent reviews on this topic [20,26,27].

In this paper we present a review of the mechanisms of ultrasound modulation of the optical signal, together with a description of the modelling and simulation methods that have been implemented probe these mechanisms. We then outline the instruments that have been constructed to detect the ultrasound modulated light. The potential for using the acoustic radiation force to increase the UOT signal strength is introduced. We then present our recent results demonstrating the potential of the acoustic radiation force for increasing the strength of the UOT signal and providing additional contrast from the mechanical properties. Representative images of a scattering and absorbing phantom illustrate the improvement in signal strength and spatial resolution over the use of pure ultrasound.

The origin of the UOT signal

Light is scattered multiple times during its passage through biological tissue, and a significant amount may be absorbed depending on the wavelength, the concentration of absorbers present (oxy- and deoxy-haemoglobin) and the thickness. If the sample is illuminated with a laser light source of sufficiently long coherence length then the intensity distribution at the output surface will be a laser speckle pattern consisting of a distribution of bright and dark ‘speckle grains’, due to the coherent summation of the random phases carried by photons that have propagated along different highly scattered path lengths [24], see Figure **1**. When ultrasound is focused into the tissue it causes a periodic compression and rarefaction of the tissue, which has two main optical effects: a modification of the local refractive index, and a modification of the position of the optical scattering sites as

illustrated in Figure **1**. Usually ultrasound frequencies of approximately 1-5 MHz are used which provides a good compromise between axial resolution and penetration depth. Photons that travel through or near to the ultrasound focus then accumulate a phase modulation through these two effects as described in the following paragraphs.

For the displacement of scattering sites, a phase modulation of the transmitted light occurs due to the change in the optical pathlengths that are modulated at the acoustic frequency [28,29]. This phase modulation results in the formation of acoustic sidebands either side of the optical frequency. Although the displacement of the scattering sites is extremely small – of the order of a few nanometres - it can be shown that strong scattering has a large effect on the output speckle field due to the accumulated effect of multiple small contributions to the change in path of the photons caused by multiple scattering events [30]. Therefore the nanometre ultrasound induced displacements of the scatterers can have a large effect on the output. From a frequency-domain perspective, the electric fields of the photons scattered by the acoustically modulated scatterers become Doppler-shifted [31], see Figure **1**.

In addition to causing the displacement of scatterers, the acoustic field also causes density fluctuations in the medium, which results in a periodic variation of the refractive index. In the case of a homogenous medium in the absence of scattering and absorption, then a collimated laser beam that is perpendicular to the acoustic field will undergo Raman-Nath diffraction from the refractive index grating, and the diffracted beams will be frequency shifted by an amount equal to the acoustic frequency [32]. In a photonic picture of this interaction, the frequency of some of the transmitted photons is shifted by the frequency of the ultrasound wave through a photon-phonon interaction. In the case of photons propagating in a scattering biological tissue, the time-varying refractive index causes a periodic modulation in the optical pathlength, which introduces a frequency shift to an optical ray passing near the acoustic focus. Note that the stronger modulation that is possible by matching the Bragg diffraction condition is generally not possible for light propagating in tissue because the scattering mean free path is too small [23]

Both of these effects (refractive index and scatterer site modulation) result in the creation of a frequency sideband in the output spectrum separated from the original wavelength by the acoustic frequency. This frequency sideband is broadened due to the other residual motions of the scatterers in the tissue [33]. The shifting of the photon frequency by twice the frequency of the ultrasound has also been observed [28], and the interaction strength has been shown to vary as the square of the ultrasound amplitude [28,29].

Modelling and simulation of UOT signals

Analytical models of the effect of the mechanisms described in the previous section on UOT signals have previously been developed for different ultrasound conditions, including continuous wave (CW) ultrasound [34], pulsed ultrasound [35], nonuniform continuous ultrasound [36] and nonuniform pulsed ultrasound [37]. These models can provide insight concerning the effects of ultrasound parameters on modulated optical signals. However, the analytical models are limited by the assumptions used. For example, typically it is assumed that the ratio of the optical transport mean free path to the ultrasonic wavelength is large so that the ultrasound induced optical phase variations associated with different scattering events are weakly correlated. This assumption is only approximately valid when the ultrasound frequency is higher than 2.5 MHz. Furthermore, it is assumed that the total phase variation due to the ultrasound modulation is very small (much less than

one radian). This condition is required so that the analytical autocorrelation function of the optical signal can be simplified, as described below. Although this may be a valid condition under normal ultrasound conditions [38] it may not be valid when high amplitude ultrasound is used. A recent simulation study [39] suggested that the total optical phase variation could be above 2π with modest ultrasound amplitude, which could lead to a possible modulation 'saturation'.

An alternative simulation method involves Monte Carlo modelling to calculate a series of photon paths through a stationary ultrasound field, which is essentially fixed in time compared to the time taken for the photons to propagate through the tissue (i.e. the simulation is carried out for one ultrasound phase) [40]. The additional optical phase accumulated along each photon path can then be calculated for the two UOT mechanisms and this can then be repeated for different phases of the ultrasound cycle by adjusting the scattering particle positions and refractive index according to the strength of the acoustic field [40]. This code can also be implemented using a graphics processing unit to rapidly calculate whole speckle images [41]. Our simulation of the optical phase of the photons as they arrive at the output face of the sample using this method is shown in Figure **2**(a). Note that this confirms that for moderate ultrasound pressures the optical phase modulation is low.

If a large number of photon paths are simulated then an autocorrelation can be calculated and the Wiener-Khinchin theorem applied to calculate the light intensity at the acoustic frequency. This method has been used to determine which of the above effects (scatterer displacement versus refractive index modification) is responsible for the majority of the modulated light under different acoustic conditions [40]. For a constant acoustic amplitude of particle displacement, the effect of increasing the size of the acoustic wave vector, k_a, is that the phase accumulated along the relatively longer optical transport mean free path is larger. Therefore the phase modulation due to the refractive index variation increases with k_a. The contribution from scatterer displacement does not vary with k_a because these displacements may be positive or negative and the sum after multiple random scatters averages to zero regardless of the size of k_a. Simulation shows that i) the contribution from the index of refraction is equal to the contribution from displacement when k_a is less than a critical fraction of the transport mean free path (0.6 μ_s from the analytical model [40]), and (ii) if k_a is greater than the critical fraction of the transport mean free path, the contribution from the index of refraction is greater than the contribution from displacement. We have simulated this in Figure **2**(b), obtaining results matched to those reported in [40,42].

Yao and Wang [43,44] further extended their simulation of UOT to inhomogeneous scattering media with a confined volume of ultrasound. As mentioned in the introduction, the transmitted intensity of light through tissue is rapidly reduced as a function of scattering and absorption and tissue thickness. It has been shown that both the AC and DC components of the transmitted light are significantly attenuated as the tissue thickness is increased. However, the AC to DC ratio – i.e. the modulation depth - decreases less significantly [43]. Since the SNR is expected to be related to the modulation depth, it should be more sensitive to changes in optical properties than the optical transmittance, and implies that UOT can detect with higher absorption sensitivity than unmodulated diffuse intensity measurements.

Note that the phases of the photons exiting the tissue are also modified by other processes in biological tissues, for instance the flow of blood which consists of moving red blood cells that may scatter the light. This movement across a whole tissue, together with other diffusions and tissue movements results in a randomisation of the optical phase and causes the rapid decorrelation of the speckle pattern, characterised by a decorrelation time τ_C. The decorrelation time is fast in tissue and

also results in a corresponding broadening of the frequency spectrum [45]. The spectral broadening from human breast tissue has been measured to be a few kHz using a method of heterodyne detection similar to those described below [46], corresponding to a τ_C of about 0.1 ms.

Methods for detecting light modulated by ultrasound

Choice of experimental geometry and parameters

To achieve a good spatial resolution, focused ultrasound transducers can be used to spatially concentrate the ultrasound field. Although the acoustically modulated photons are generated with equal probability along the ultrasound axis, there is a relatively increased signal from optical absorbers within the ultrasound focal region. In order to improve the axial resolution a number of further developments are required as described in the 'methods of scanning the object' section below. Ultrasound frequencies used are in the range of 1-5 MHz to provide a good tissue penetration and a small focal volume (~300 microns diameter, 9 mm depth of focus for 5 MHz ultrasound). There are many different geometries with which UOT signals may be detected, but in general, for convenience, the ultrasound and optical axes are often perpendicular to each other and the light is detected in transmission, e.g. [47]. There are also reflection geometries, for instance [48], [49] and [50], and side-detection configurations [51] which may be advantageous for detecting signals from very thick tissues where transmission detection may not be possible. Granot et al. have developed an analytical solution to express the strength of the signal and the signal to noise ratio as a function of the ultrasound focal position [52].

When choosing a light source for UOT experiments one of the main considerations is the requirement that a sufficiently long coherence length laser must be used with a high enough power to be able to yield enough photons transmitted (or reflected) from the sample. Monte Carlo modelling can again be used to simulate the propagation of many random photon paths through the tissue based on the simulated optical properties. Photons that are not absorbed in the simulated tissue can be traced to one of the output faces, allowing various useful parameters to be studied, for instance the pathlength distribution of the light [53]. For a 3 cm thick tissue, it is found that the range of pathlengths within 50% of the mode pathlength is around 7 cm (i.e. the pathlength distribution spans ~3-10 cm in the tissue). Therefore in order to maintain a clear speckle pattern on the output tissue face, the coherence length of the laser source should be approximately 7 cm or more [54].

This has led to the widespread use of 532 nm (frequency doubled Nd:YAG) lasers, although these are not optimal for obtaining good transmission, since the tissue optical transmission region is in the red and near infrared spectral region. Therefore some groups have used single mode laser diodes in the red [48] or near infrared [12], HeNe [49] and Ti:sapphire [55] lasers. More complex pulsed systems have been demonstrated, including a Nd:YAG ring oscillator amplifier [56] for increasing the optical detection efficiency. The light may illuminate a large region of the sample (~cm diameter) [12] or alternatively small single fibre input may be used [48]. The choice of light source may also be determined by the operating wavelength of the optical detection device, for instance the appropriate wavelength for a photorefractive crystal or a spectral filter. Multiple wavelengths have also been used to allow more quantitative tissue absorption measurements to be made [57,58]

Single point detection methods

Early detection methods typically used a single point detector that was either a similar size to one of the optical speckle grains or integrated over a number of these speckles. The two main detection

methods may be classified as either heterodyne or interferometric. In heterodyne detection, a part of the illuminating laser is split and recombined with the signal beam at the detector, producing a temporal modulation as a result of the frequency shifted signal beam. In the case of UOT, rather than splitting a part of the input beam, the heterodyne detection may take place between the light that was modulated at the ultrasound focus and that which did not pass through the focus. The speckles that are formed from the scattering of the light in the sample are uncorrelated with each other and so the largest modulation depth is obtained with the signal is collected from only one speckle grain, which severely limits the etendue. The second method (interferemetric detection) combines the signal beam with itself using an optical filter or interferometer (Mach-Zehnder) [59]. It is not possible to separate the frequency-shifted light from the background unmodulated light using standard optical filters for UOT, but it is possible to use a Fabry-Perot interferometer to selectively detect the frequency shifted light [60].

Fast photodetector and electronic filtering

The early reports on detecting the ultrasound modulated light used single point detectors [14,47,61] such as photodiodes or photomultiplier tubes (PMTs) that were able to detect both the unmodulated and the ultrasound modulated light in a configuration similar to that shown in Figure **3**(a). Electronic filtering could then be used to determine the amplitude of the AC component of the detected signal and thereby give an indication of the amount of light absorbed at the focus of the ultrasound transducer. An aperture was usually placed outside the sample and in front of the detector in order to control the size of the optical speckle so that it was approximately the same size as the detector. In a slight variation a part of the incident laser light can be picked off before the sample and then recombined with the signal beam at the photodiode [29]. This laser light then provided a local oscillator and the signal was found by filtering the output from the photodiode at the ultrasound frequency.

With this fast detection method the detection time can be within the speckle decorrelation limit, i.e. the total acquisition time must be much less than the time required for the speckle pattern to be affected by other processes such as the motion of blood cells or tissue motion [14]. Often, due to the weakly modulated signals, a compromise must be made between an improvement of the signal to noise ratio (SNR), through increasing the number of photons detected, and a reduction in the SNR, through speckle decorrelation [54].

Use of FP interferometer

Since the detection of the ultrasound modulated light involves a frequency shift of the optical frequency by the ultrasound frequency, detection schemes have been proposed that can optically filter the unmodulated light so that the full dynamic range of the detector may be used. This overcomes the well-known problem of trying to detect a small signal on top of a large DC background carrying shot noise, i.e. it is better to detect the signal in a darkfield configuration.

One method to achieve this is to use interferometric detection with a confocal Fabry-Perot interferometer (CFPI), which is able to efficiently filter the background unmodulated light [62,59], Figure **3**(b). This idea, along with a number of others that are currently used in UOT, originally came from the detection of surface deformations as a result of acoustic modulation of the sample as a means of material inspection. Sakadžic et al. used a high frequency (15 MHz) high resolution pulsed UOT system that incorporated a CFPI that was tuned to the laser frequency plus 15 MHz. This filtered out the background light achieving a measurement resolution of less than 100 microns at 3 mm tissue depth. The high intensity of the ultrasound pulses was able to overcome the noise limitation of the

large bandwidth. CFPI can achieve a large etendue and is not affected by the decorrelation of the speckle (since they operate with incoherent light at fixed transmission frequencies). One limit is that the rejection of the background light is more efficient for higher ultrasound modulation frequencies and so the use of CFPI may be best suited to achieving high resolutions in thinner tissue samples. This has more recently been demonstrated in a technique for ultrasound-modulated optical microscopy, where acoustic frequencies of up to 75 MHz were used to achieve an axial and lateral resolution of 30 and 38 μm [63]. Such a high resolution (but at low imaging depth) has possible applications in detecting sentinel lymph nodes using an absorbing contrast agent [18] or for monitoring sub-surface vasculature [64].

Spectral hole burning

A technique for spectral filtering to leave only the light that has been frequency shifted to an acoustic sideband has recently been proposed by Li et al. [82] as an alternative method to the use of a confocal Fabry-Perot interferometer. The principle is that frequency shifted light is transmitted by a spectral hole burning crystal (a rare-earth ion doped optical absorber). This has a two level atomic energy level structure and is inhomogeneously broadened, meaning that specific atoms have slightly different transition wavelengths. If it is cryogenically cooled then the (homogeneous) broadening of these transitions is sub megahertz [82]. When illuminated with light at an energy that is equal to one of the transitions, the crystal will absorb the light and subsequently reradiate it as fluorescence. If a sufficiently high power laser is used, all of the atoms at a particular transition energy may become excited, causing saturation and relative transparency to additional photons at that wavelength.

For making UOT measurements a high power pump laser is frequency shifted to the ultrasound-modulated frequency sideband, and is used to burn a spectral hole in the crystal. The signal photons are then transmitted through the crystal while the unmodulated background light is absorbed (see Figure **3**(g)). These crystals may be used at around 800 nm and are therefore well matched to the tissue optical transmission window. In the experiments reported the pump light is pulsed by activating an AOM so that a spectral hole may be burnt before the signal light arrives (the spectral hole filter lifetime is approximately 10 ms). Even though a speckle pattern is formed at the detector, the signal information is contained in the intensity of the light, and the detector may therefore integrate light from multiple speckles simultaneously and a high etendue may be achieved. The signal strength then increases with the square root of the number of speckles [24], and that speckle decorrelation does not affect the signal as the detection is incoherent. An axial scan may be achieved by resolving the photodetector intensity as a function of time during pulsed ultrasound propagation, and further work on the modelling of these crystals has been presented in [65].

Parallel detection

The low light level present in a single speckle limits the detection time. Kempe et al. calculated that the signal to noise ratio would not be high enough for breast tumour diagnosis due to the shot noise limit [29]. Gross et al. considered the efficiency of detection in terms of the optical etendue (the product of the solid angle of the light emission or collection with the active area) of the typical light collection schemes used [66]. For the emitting surface of the sample the etendue is πA whereas for a single speckle grain the collection etendue is approximately λ^2. Therefore the collection efficiency for typical UOT systems was calculated to be about 10^{-10} for a single pixel and 10^{-4} for parallel detection with 10^6 pixels. The light collection efficiency can be improved by increasing the detection area, and the DC component will increase in direct proportion to this. However, since the phases of different speckles are uncorrelated the increase in detected modulated photons will be countered by an averaging out of the modulation. The DC component increases more rapidly than the AC component

as the detection area is increased, reducing the modulation depth by the square root of the number of speckles contained within the detection area [28,54]. In reality there is a trade-off because neighbouring speckle grains are not necessarily completely uncorrelated, and there is also the noise characteristic of the detection system to take into account [29,61].

It is desirable therefore to simultaneously maximise the detection of the modulated signal by using multiple detectors that are of a similar size to the speckle grains, leading to the use of imaging detectors. However, the use of imaging technology imposes a maximum frame rate of 100's to 1000's Hz on the detection - not fast enough to directly detect the MHz optical modulation electronically – and various schemes have been proposed to detect the modulated light. These may be classified as:

- Analysis of the spatial statistical properties of the speckle;
- Parallel lock-in speckle detection; and
- Heterodyne detection using digital holography.

These methods are described in the following sections, together with a technique that combines some of the principles of these methods – detection using photorefractive holography.

Laser speckle

The possibility to use properties of the optical speckle pattern that is formed when a laser (with a sufficiently long coherence length) is passed through an ultrasound modulated scattering medium was proposed by some early patents in this field e.g. [67]. Essentially, if the distribution of scatterers in the sample is stationary then the speckle interference pattern on the CCD is stationary. However, if the scatterers move on a timescale similar to the CCD exposure time, the camera records a moving speckle pattern, which causes the speckle grains to become blurred (see Figure **3**(c)). The degree of blurring can be determined by measuring the contrast of the image [68], which is correlated with the number of photons that have been modulated by the ultrasound. The first demonstration of this technique in UOT was by Li et al. in 2002 [69]. In these experiments, chicken breast of up to 25 mm thickness was imaged with gizzard inclusions. A low degree of speckle contrast was recorded (0.14) because no analyzing polarizer was used and the speckle size was reduced to less than the size of one pixel to allow more light to be detected. This resulted in a low contrast difference for less absorbing inclusions.

This approach has an advantage over the other parallel detection methods in that only one image of the speckle pattern needs to be recorded and therefore the problem of sample movement and speckle decorrelation may be reduced, although the signal is reduced for long camera exposure times depending on the ratio of the decorrelation time to the exposure time. This method is the basis of the experiments reported later in this paper.

Parallel lock-in detection

An alternative approach uses parallel lock-in detection to allow the ultrasound-induced optical modulation to be determined for every pixel in a CCD array. The original scheme was proposed by Gleyzes et al. [70] and a system was constructed by Leveque-Fort et al. that incorporated a 256x256 CCD array that was read at a frame-rate of 50 Hz [12]. The illuminating laser diode was modulated at the same frequency as the US, and four 20 ms frames were read from the camera for different relative phases between the ultrasound and laser (see Figure **3**(d)). From these images the amplitude and phase of the modulated light could be calculated for each pixel. However the signal is reduced over the period of the four-frame measurement due to speckle decorrelation.

Heterodyne parallel speckle detection

As described above, one of the problems faced by methods to detect the modulated (signal) photons is that the signal is weak and sits on a large background. This leads to the requirement of large dynamic range detectors and even then the background noise will be large compared with the signal strength. An imaging method was proposed by Gross et al. [71] that is able to counter this problem through the use of heterodyne holography [72]. In this scheme, part of the laser is split from the main beam before it enters the sample in order to act as a reference local oscillator beam (as illustrated in Figure **3**(e)). If the local oscillator is then frequency shifted by the ultrasound frequency using an acousto-optic modulator (AOM) (since the required shifts are small a pair of AOMs is usually used to shift up and then down by slightly different amounts) it can be recombined with the signal beam to produce interference between the local oscillator and the signal. An important principle of this technique is that the strength of the modulation depends both on the intensity of the signal and on the intensity of the local oscillator. Therefore by increasing the strength of the local oscillator, the amplitude of modulation may be increased, which carries information on the intensity of the signal. Therefore the signal may be amplified above the camera read noise by the local oscillator without any background amplification and can become shot-noise limited [71].

To detect the modulation, a number of modifications are made to the schematic described above [71]. Specifically, the local oscillator frequency is shifted slightly higher than the acoustic frequency ($\nu_s + \nu_{CCD}/4$) to allow multiple images (typically four) of the interference pattern to be recorded on the CCD that have different phases between the signal and local oscillator. The modulation depth can then be calculated on a per pixel basis by using a simple calculation [73] based on the four input images (refer to Figure **3**(e)).

A second modification is that a narrow aperture is inserted close to the sample surface, which increases the size of the speckle grains produced from the self interference of the sample photons. Thirdly, the reference beam is incident on the CCD from an angle slightly offset from the signal beam. This shifts the spatial frequencies that are carrying the interference information between the local oscillator and the signal beam to higher values and this can allow them to be distinguished from the low frequency sample speckle. The speckle hologram may be Fourier transformed to allow the important spatial frequencies relating to the signal light to be selected and the speckle decorrelation noise to be filtered out [71]. The effect of speckle decorrelation during the acquisition time for this technique is therefore reduced both due to the shorter acquisition times achievable due to the heterodyne gain, and the reduction in the speckle decorrelation noise.

Photorefractive crystals

Again inspired by detection methods that are used in the optical study of acoustic surface effects for materials inspection [74], the use of photorefractive crystals was proposed [75,76]. This method allows the signal contribution for each speckle to be integrated on a single detector by using a holographic method that matches the reference beam wavefront to the complex speckled wavefront leaving the sample. The resulting increase in signal strength then allows a higher signal to noise ratio to be achieved over single speckle measurements.

Photorefractive materials exhibit an optically induced change in refractive index (and/or absorption) in response to spatially non-uniform illumination. Fundamentally, the change in refractive index is due to an internally varying electric field that is created by photo-excitation of charge in response to the spatially varying incident illumination. The spatial variation in illumination gives rise to charge transport and trapping within the photorefractive medium. The resulting spatial modulation of the

electric field is then converted into a change in refractive index through the electro-optical properties of the photorefractive e.g. via the linear Pockels effect [77], creating a holographic refractive index pattern that can then cause diffraction of light. In the case where two beams are incident on the crystal (a signal and reference beam), the refractive index grating can diffract some of the signal beam so that its wavefront is then matched with the reference beam. The result is that the random phases that are present in the speckle from the signal beam disappear and a low etendue single 'pixel' detector can then be used. The etendue of the whole detection system is then defined by the size and resolution of the photorefractive crystal employed. This combines the advantages of large area etendue detection without reducing the modulated signal by averaging out the modulation.

There are two main methods used for detecting the modulated light in practice. The first of these uses part of the illuminating beam as the reference light [75], which results in a refractive index grating being written by the unmodulated photons. The reference beam is then diffracted into the signal beam path and is wavefront matched to the unmodulated light, which is then amplified at the detector. Although only the unmodulated light is amplified, the changes in the DC offset of this signal can be used to infer the amount of light that is modulated.

The second method (illustrated in Figure **3**(f)) uses a frequency shifted reference beam so that only the small modulated component writes the refractive index grating. The diffracted light from the reference beam is wavefront matched to the modulated light and a photodetector records the transmitted light with a heterodyned amplified modulated component (for more details on this mechanism see the heterodyne parallel detection section above). These two methods have been theoretically studied to determine the mechanisms of signal detection [78,31], and it has been suggested that the second method has advantages as it is effectively a background free detection technique [79] although no clear advantage has yet been conclusively demonstrated.

There are a number of disadvantages with the photorefractive crystal methods, particularly that the spectral response currently limits their use to longer infrared wavelengths, away from the region of low tissue absorption in the red and near infrared. However, recently a tellurium-doped tin thiohypodiphosphate (SPS:Td) ferroelectric crystal was used at 790 nm, which holds promise for applying photorefractive crystals at the optical tissue window where water absorption is lower [80]. Also, the refractive index grating can only track the decorrelation of the speckle pattern caused by sample motions provided that the photorefractive response time is sufficiently fast [56], otherwise the signal is modified depending on the ratio of the decorrelation time to the photorefractive response time. It has recently been reported that a GaAs photorefractive crystal could achieve a response time of 0.25 ms, which is about the same value as the speckle decorrelation time for thick tissue [81]. Another disadvantage is that light from the strong reference beam may also be scattered and provide a high background light level at the detector [82].

Tissue phantoms

When phantoms are used, effort is taken to try to match the optical absorption and scattering parameters as closely as possible to tissue. Many different types of simulated biological tissue have been used for UOT, including water with trypan blue (absorber) and polystyrene beads (scatterer) [47], gelatine with trypan blue [61], agar with intralipid and Indian ink [83] or chicken and turkey breast tissue [12]. The first *in vivo* demonstration of UOT was by Lev et al. [84] who studied the light that was backscattered from a mouse and also a human forearm. This was collected by an optical fibre and detected by a PMT. This study illustrated that the speckle decorrelates much faster than in most tissue phantoms studied due to the scattering by moving tissue components, for instance red

blood cells flowing in the microvasculature, and the unrealistic speckle decorrelation times remain a limitation of phantom based studies.

Methods of scanning the object

The most simple method to build up a three dimensional map of the UOT signal is to physically scan the sample [47, 61], or to move the ultrasound transducer [29]. In order to reduce the amount of scanning that is required to create two and three dimensional images of the sample and to provide axial (z-axis) resolution, Wang and Ku used a frequency-swept ultrasound beam [21]. By simultaneously modulating the PMT with a frequency-swept gain, different points along the ultrasound axis could be resolved due to their different heterodyne frequencies in the output electronic signal. A Fourier transform of this waveform could then allow the ultrasound modulated optical signal to be resolved into different frequencies corresponding to different positions along the ultrasound axis. This method also improved the spatial resolution because if the whole ultrasound column was to be simultaneously modulated at the same frequency then light interacting with the ultrasound anywhere inside the affected volume may be modulated [54].

The frequency swept (chirped) approach also helps to improve the limited spatial resolution that can be achieved in the ultrasound propagation direction. Typical focused ultrasound transducers that are used in the MHz frequency range at few cm focal depths have focal regions that have resolutions of <1 mm laterally and 10 mm longitudinally [85]. The chirped pulse methods can allow the photons traversing different regions of this ultrasound focus to be resolved.

The chirped frequency scheme was initially only used with a single detector for detecting ballistic photons due to the limited signal to noise ratio that could be achieved, although it was subsequently expanded to exploit the parallel detection of multiple speckles using lock-in detection and a CCD (Figure **3**(d)). This was achieved by modulating the laser with a frequency-swept signal and simultaneously modulating the ultrasound with the same frequency-swept signal at a specific *delay* relative to the laser [86]. This delay time determined the spatial location along the ultrasound axis at which the lock-in method was effectively being applied, thereby achieving z-axis resolution. Chirped ultrasound and imaging [21 and 86] were subsequently combined by modulating the laser with a frequency-swept signal and simultaneously modulating the ultrasound with a frequency-swept signal at a constant *frequency* offset relative to the laser [87]. Heterodyne detection was then achieved at the CCD, and the signal from different spatial locations along the ultrasound axis could be found by calculating the FFT on a pixel-by-pixel basis since the frequency spectrum simply encoded the z-axis location. One of the limits of this technique is that the scatterers in the sample must be stationary over the whole period of the chirp, i.e. there must be no decorrelation of the speckle pattern during the acquisition, which in this case was around two seconds. An alternative method that also provides axial resolution uses a random series of phase jumps in the ultrasound signal that is replicated and also applied to the optical signal. By varying the delay between the application of these two signals and using a photorefractive holographic readout scheme, a specific ultrasound axial position may be isolated [88].

The use of computer tomography methods has been proposed to further increase the optical resolution by overcoming the limit of the relatively long longitudinal ultrasound depth of focus (~10 mm). The UOT signal detected can be considered as an integration of many incremental contributions from different points along the ultrasound axis. This is conceptually similar CT imaging and by rotating and translating the object and recording multiple projection angles, Radon transform methods could be used to make a reconstruction of the object [16].

Short ultrasound pulses can also provide z-axis resolution by recording the output AC optical signal with a high temporal resolution [49] as the pulse propagates. The use of pulses also allows for lower acoustic doses to be used that are in line with medical safety limits whilst maintaining the peak power, which is more standard for medical ultrasound systems. Since a high detector temporal resolution is required, this method cannot be easily incorporated into the imaging methods described previously, although a stroboscopic approach can be used. For instance Atlan et al. used the heterodyne holography method and showed that by stroboscopically activating the local oscillator they could resolve UOT data as the ultrasound pulse propagated through the sample [89].

An alternative method for obtaining resolution along the transducer propagation direction proposed by Selb et al. [85] used the detection of nonlinear effects as the incident ultrasound power was increased. The optical modulation at the second harmonic was studied, which is expected to occur where the peak powers are high due to nonlinear processes, or from the interference of two waves that are both phase shifted at the ultrasound fundamental frequency which causes interference at the second harmonic. It was suggested that this interference effect may be the dominant contribution due to the experimental observation that the second harmonic optical modulation intensity increased with a quadratic dependence on the ultrasound power [85]. The signal detected at the second harmonic had a higher contrast and a better spatial resolution than the fundamental.

Spatial resolution can also be obtained by integrating UOT methods with standard ultrasound instruments. The efficient detection methods that are employed using the photorefractive crystal approach in particular has allowed images acquired with the standard ultrasound mode to be overlaid on images that were acquired using UOT so that automatically co-registered ultrasound/UOT images could be displayed [90].

There are a number of factors that cause spatial variation in the UOT signal that must be accounted for when scanning three dimensional phantoms. When considering the standard UOT set-up as depicted in Figure **1**, it can be shown using Monte Carlo modelling that as the ultrasound focus is scanned along the y-axis from the light source towards the camera, the UOT signal strength decreases. This is due to the higher relative numbers of photons that are modulated at the light input face which gives a higher signal to background ratio [54]. The ultrasound signal strength also decreases as the ultrasound probe is scanned in its axial direction as a result of the acoustic attenuation of the sample. It should also be noted that an increase in the spatial resolution may decrease the SNR of the already weak UOT signal.

Attempts to increase UOT signal using the acoustic radiation force

The ultrasound displacement of scatterers is typically in the range of a few nanometres for clinically compatible ultrasound frequencies and intensities. The low optical modulation depth of the UOT techniques could potentially be increased by achieving larger scatterer displacements and therefore a greater modulation depth (until the signal saturates). One method of achieving this is to use the acoustic radiation force instead of the pure ultrasound, which can cause tissue displacements of a few microns [91,92].

When ultrasound waves are attenuated, i.e. absorbed, reflected, or scattered by a medium, a small and unidirectional force can be generated within the medium which is called acoustic radiation force (ARF). This is caused by the small momentum transfer from the ultrasound beam to the medium [93]. The amplitude of ARF depends on the amplitude of the ultrasound, the attenuation coefficient of the

medium, and the cross-sectional area of the ultrasound beam. A common method to control the ARF is to alter the amplitude of the ultrasound, for example a transient ARF can be generated by an ultrasound impulse, while an oscillatory ARF can be obtained by amplitude modulating the ultrasound. Another parameter which affects ARF is the frequency of the ultrasound, since the tissue attenuation is roughly proportional to the ultrasound frequency. However, although the ARF in regions close to the transducer increases with higher ultrasound frequencies, the amplitude of ultrasound is more quickly attenuated and hence after a certain depth ARF is be reduced.

Although the first measurement of the ARF was made as early as 1903 [94], only recently has this physical phenomena been widely explored in biomedical sensing and imaging applications. Nightingale et al. [95] were among the first to demonstrate the potential of measuring the ARF in vivo when they induced streaming within cysts to distinguish them from solid lesions. Sarvazyan et al. [91] demonstrated the potential of ARF in imaging tissue elasticity properties, using the ARF to remotely induce shear acoustic waves which could then be measured to obtain tissue mechanical properties in a technique called shear wave elasticity imaging (SWEI). The measurement of the tissue displacement due to the shear wave was made using an optical system and an MRI scanner, although it could be possible to use the same ultrasound transducer. In the same year Fatemi et al. [96] proposed a similar technique to probe tissue properties using an oscillatory ARF generated by interfering two focused ultrasound beams (ultrasound-stimulated vibro-acoustic spectrography). The measurements were made with a separate acoustic sensor which was sensitive to the kHz frequencies of the ARF oscillation. Calcification on *ex vivo* human artery was clearly detected and visualised and the system demonstrated a reasonable spatial resolution of 700 μm. Nightingale et al. [95] reported a clinical feasibility study to image tissue elasticity of various tissues using transient ARF, where short (<1 ms) focused ultrasound was applied and the resultant tissue displacement was measured using an ultrasonic correlation-based method. It has been demonstrated that tissue displacements on the order of 10 μm can be generated by ARF. More recently, the use of the ARF has been integrated into a clinical ultrasound scanner for 'supersonic shear imaging' which provides quantitative elasticity measurements that potentially could help in breast lesion characterisation with B-mode ultrasound [97].

A few methods have been proposed to generate an ARF in UOT, including the use of short intense bursts of ultrasound [98,99,100,25] as well as amplitude modulated ultrasound [39,55] and beating between two confocal ultrasound transducers [101]. These methods produce a time varying intensity to the sample which causes a time varying displacement of the scatterers. This displacement also depends on the acoustic absorption and reflection properties of the sample, since these both produce changes in momentum in the ultrasound wave, with high reflecting and absorbing samples producing a higher ARF. The final particle displacement therefore depends both on the ultrasound strength, the local absorption or scattering and the local shear stress. An additional effect that results from the ARF is that shear waves are produced that propagate away in a direction perpendicular to the ultrasound direction [102]. The advantages and limits of using the ARF will be discussed in more detail in the final section below, summarising our recent observations.

Use of ARF to detect optical and mechanical contrast

We have previously studied the trade-off in the use of the ARF between spatial resolution and signal strength when using an amplitude modulated (AM) ultrasound trace to generate a periodically varying ARF in a tissue mimicking phantom [103] using the set-up illustrated in Figure **4**. The phantoms used were made of agar with intralipid to provide an optical scattering coefficient of 5 cm^{-1} and Indian ink

to absorb the light. Although these phantoms did not have any specific ultrasound absorber or scatterer added, the high ultrasound frequency used (5 MHz) resulted in sufficient ultrasound absorption and a detectable ARF. The AM frequency was 500 Hz and CCD images were recorded with two different exposure times (0.2 ms and 2 ms). These were found to be sensitive either to pure ultrasound modulation (0.2 ms exposure) due to the small distance that the optical scatterers moved during this low integration time, and the ARF (2 ms exposure). A delay generator was used to record speckle images of the scattered light field at different delay times with respect to the initiation of the ultrasound pulses (see Figure **4**). Different inclusions with varying mechanical and optical absorption properties were inserted into the phantoms so that the sensitivity to these objects could be studied for the two regimes (0.2 ms and 2 ms exposure times). Illustrative results are presented in Figure **5** and Figure **6**.

Figure **5**(a) shows that results recorded at different delays after the start of an AM signal burst for a phantom that had an absorbing cylindrical inclusion (6 x 6 x 4.3 mm) within it. This shows that when the ultrasound beam is focused just outside the absorbing region the UOT signal (in this case ΔC, the change in speckle contrast, which gives a positive value when the ultrasound focus is not in an absorbing region) when using the 2 ms CCD exposure time is much higher than that for the 0.2 ms exposure time (the two red curves). This implies that sensitivity to the ARF leads to a higher UOT signal strength. However, besides the increase in UOT signal due to large ARF-induced movement of the scatterers, the ARF also leads to a shear wave propagating away from the ultrasound focal region. This shear wave also causes significant displacement of optical scatterers and contributes to the change in contrast observed, although it results in a worse spatial resolution.

When the ultrasound focus was located inside the absorbing region of the phantom (blue lines in Figure **5**(a)), there was no UOT signal from the 0.2 ms CCD exposure time, as expected. For the 2 ms exposure time, there was initially no UOT signal since the light that passes through the ARF affected region is absorbed. However, the shear wave propagation resulted in a signal being recorded a few ms later, which we attribute to the shear wave propagating out of the absorbing inclusion.

Figure **5**(b) shows a time course of the evolution of the 1D UOT scan data as the phantom is translated across the ultrasound beam. This shows that the spatial resolution and signal strength were highest at about 1 ms after the launch of the acoustic burst and at later times the propagation of the shear wave caused a blurring of this signal. The result for the 0.2 ms CCD exposure time is also included, showing a 40% improvement in spatial resolution and a ~100% improvement in image contrast when the ARF was used.

To demonstrate that the acoustic radiation force may be used to detect the mechanical properties of the sample a phantom was constructed that had an optical absorption and a mechanical discontinuity (made by adjusting the concentration of agar [83]), which had a lower shear stiffness, as illustrated in Figure **6**(a). The two CCD exposure times (0.2 and 2 ms) were used to record speckle images, and the change in UOT contrast for a one dimensional scan across the phantom is illustrated in Figure **6**. The red line was recorded for 0.2 ms exposure time and shows that the standard ultrasound was able to detect the optical absorbing inclusion, but not the inclusion with a different shear stiffness. However, the 2 ms exposure time has a sensitivity to the ARF and also to any shear wave produced. The change in stiffness results in a modification to the shear wave produced and the system is therefore sensitive both to the optical and the mechanical inclusion.

2-D images were recently measured with the same CCD exposure times (0.2 and 2 ms) and the same trigger delay times on a phantom containing an optical absorber (dimension 5 x 5 x 5 mm) by scanning the phantom. The results in Figure **7**(a) and (b) show 2-D images captured with a 0.2 ms CCD exposure time and a 2 ms CCD exposure time respectively. The full width half magnitude (FWHM) of the absorbing region was 6 mm for the ARF-sensitive 2 ms CCD exposure time and the FWHM was 7 mm for the traditional non-ARF signals measured with the 0.2 CCD exposure time. This represents an improvement of more than 17% in spatial resolution. The differences in contrast between the maximum and the background were ~0.059 and ~0.0423, respectively, which is a 40% improvement in image contrast for the ARF modulated signals compared with the pure ultrasound modulated signals. The spatial resolution and image contrast of the 2-D image does not increase as much as the 1-D result due to the geometric difference between the phantoms.

The spatial resolution and image contrast of the 2D images measured with the short CCD exposure time (0.2 ms) do not change with time. However, when using the longer CCD exposure time (2 ms) and different CCD delay times (1 ms, 5 ms, 9 ms and 13 ms), the spatial resolution of the 2-D images decreases from a maximum at 1 ms. These results again demonstrate that short CCD exposure times tend to filter lower frequency vibrations from the ARF and are only sensitive to high frequency movements at the ultrasound frequency. When using the longer CCD exposure time, the effects of low frequency movements induced by ARF and resulting shear wave can be detected. With the optimal trigger delay time, the spatial resolution and image contrast can be improved simultaneously compared with pure ultrasound.

The increase in signal strength that can be obtained by using the ARF to make UOT measurements therefore has to be carefully balanced with the possible loss in spatial resolution due to the propagation of the shear wave. The timing of the signal acquisition after the generation of the ARF should be kept as short as possible, and consideration should be made of the dependence of the attenuation of the shear wave as a function of ultrasound frequency. A potential additional benefit of the ARF is that it allows the simultaneous probing of the optical and mechanical properties of the tissue, since the signal strength is also affected by the stiffness of the tissue [83,103]].

Conclusions

UOT has been shown to be sensitive to a number of tissue parameters, including the local absorption and scattering properties at the ultrasound focus, the ultrasound absorption, the material shear stiffness and the shear wave attenuation. The measurement of these parameters either individually or in a combination would potentially provide a useful diagnostic signal for medical applications of this technique. The sophisticated detection techniques that have been developed to detect the weak UOT signals include the use of high finesse interferometers, photorefractive crystals, spectral hole burning crystals and heterodyne holographic techniques. These methods have demonstrated the potential for detecting sentinel lymph nodes, microvasculature, gold nanoparticles and for monitoring ultrasound therapy. The possibility of using multispectral methods to quantitatively and non-invasively detect these signals at depths of a few cm and with mm resolution has potential for breast cancer imaging due to the possible sensitivity to tumour metabolism through the detection of oxygenation levels. At present the translation of this technology into a clinically relevant diagnostic device has been slow. The combination of better detection methods, higher UMT signals from the use of alternative ultrasound modalities, and the possibility of probing the optical and mechanical properties simultaneously can be expected to open up further niche applications for these methods.

Acknowledgements

The authors would like to thank the UK EPSRC (Grant numbers: EP/H02316X/1 and EP/E06342X/1) and the Royal Society for their financial support. DSE is supported by European Research Council Starting Investigator Award 242991.

Figure captions

Figure 1: Schematic showing the propagation of representative highly scattered photons through a biological tissue in the presence of a focused ultrasound beam. The resulting speckle pattern at the output face is illustrated together with the modulation in intensity of a single speckle grain. Note that the scattering is low in this illustration resulting in a well defined optical beam, and that no absorbers are included.

Figure 2: (a) Results from a simulation of a UOT system showing the phase shifts $\boldsymbol{\varphi_j}$ for 9103 detected photons for a focal pressure of P_{focal}=2 MPa and k_a of 2.1×10^4. The histogram bins have a width of 2 degrees. (b) The speckle pattern modulation depth contributed by the index of refraction alone, M_n; the modulation depth contributed by displacement alone, M_d; and the modulation depth contributed by both, M_{sum}. The Monte Carlo simulation is based on [40].

Figure 3: Summary of the main methods used to detect UOT signals. (a) Photodetector measurement, (b) confocal Fabry-Perot interferometer detection, (c) speckle image contrast analysis, (d) lock-in image detection, (e) heterodyne holographic detection, (f) detection using a photorefractive crystal, (g) spectral hole burning detection. PD – photodetector, AOM – acousto-optic modulator, PR – photorefractive crystal, ν_O - optical frequency, ν_{US} - ultrasound frequency, ν_X – frequency shift (typically ~ 70-80 MHz), ν_{CCD} – CCD camera frequency.

Figure 4: Experimental set-up. FG – frequency generator, US – ultrasound transducer. The trigger timing controlled by a Stanford DG535 is also illustrated showing: T1 - triggering the CCD camera when the ultrasound is off, T2 - triggering the function generators to produce the ultrasound signal, T3 - triggering the CCD camera when the ultrasound is on. The UOT signal is found from the difference in contrast between the two CCD exposures.

Figure 5(a) Contrast difference versus CCD trigger delay time for a 250 Hz-AM ultrasound burst with 0.2 ms and 2 ms CCD exposure time in a homogeneous area (blue line) and an absorbing area (red line) (b) Comparison between a 1-D profile of an optical absorber obtained with a 0.2 ms CCD exposure time measured 2 ms after launching a 250 Hz-AM acoustic burst (red line) and 1-D profiles with a 2 ms CCD exposure time measured at varying delay times after launching a 250 Hz-AM acoustic burst (Reproduction permission to be obtained from [103]).

Figure 6: (a) Illustration of the phantom and a photograph of the cross-section taken after the experiments. The diameter of the Indian ink optical inclusion (on the left) was ~3.5 mm. The diameter of the stiffer inclusion (on the right inside the red-dashed circle) was ~8 mm. (b) B-mode ultrasound image of the phantom in the Y-Z plane showing no contrast from the optical or mechanical inclusions. (c) 1-D profiles of the inhomogeneous phantom measured with various CCD exposure times and CCD delay times. Again the optical inclusion was on the left and the stiffer inclusion was on the right. (Reproduction permission to be obtained from [103])

Figure 7: (a) A 2-D profile of an inhomogeneous phantom measured with a 0.2 ms CCD exposure time and a 2 ms CCD trigger delay time. (b) A 2-D profile of an inhomogeneous phantom measured with a 2 ms CCD exposure time and a 1ms CCD trigger delay time. (c) 1-D profiles taking along the midline (Z = 9 mm) from (a) and (b). (d) 1-D profiles taking along the midline (Y = 0 mm) from (a) and (b).

Figures

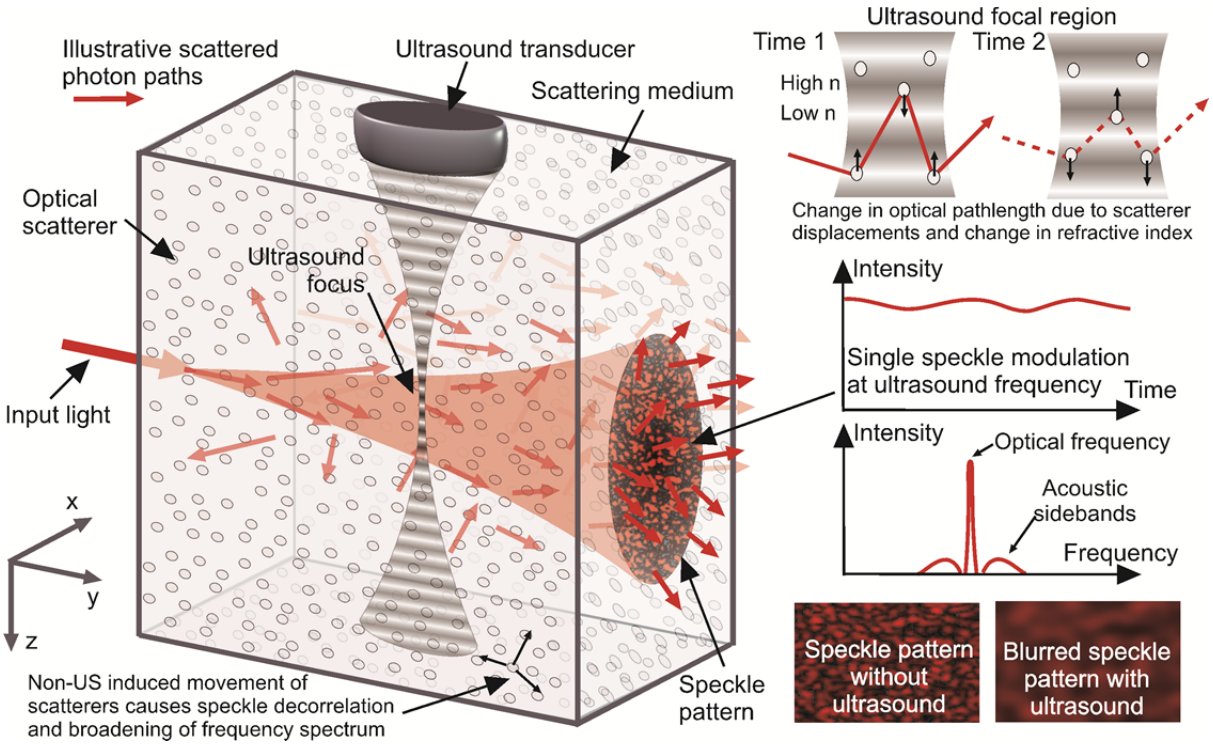

Figure 1: Schematic showing the propagation of representative highly scattered photons through a biological tissue in the presence of a focused ultrasound beam. The resulting speckle pattern at the output face is illustrated together with the modulation in intensity of a single speckle grain. Note that the scattering is low in this illustration resulting in a well defined optical beam, and that no absorbers are included.

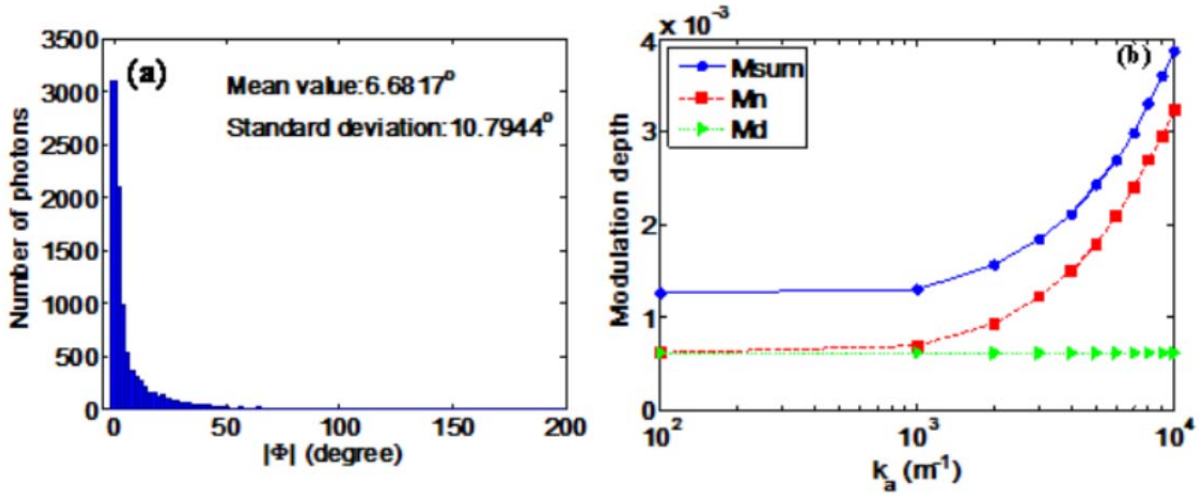

Figure 2: (a) Results from a simulation of a UOT system showing the phase shifts φ_j for 9103 detected photons for a focal pressure of P_{focal}=2 MPa and k_a of 2.1×10^4. The histogram bins have a width of 2 degrees. (b) The speckle pattern modulation depth contributed by the index of refraction alone, Mn; the modulation depth contributed by displacement alone, Md; and the modulation depth contributed by both, Msum. The Monte Carlo simulation is based on [40].

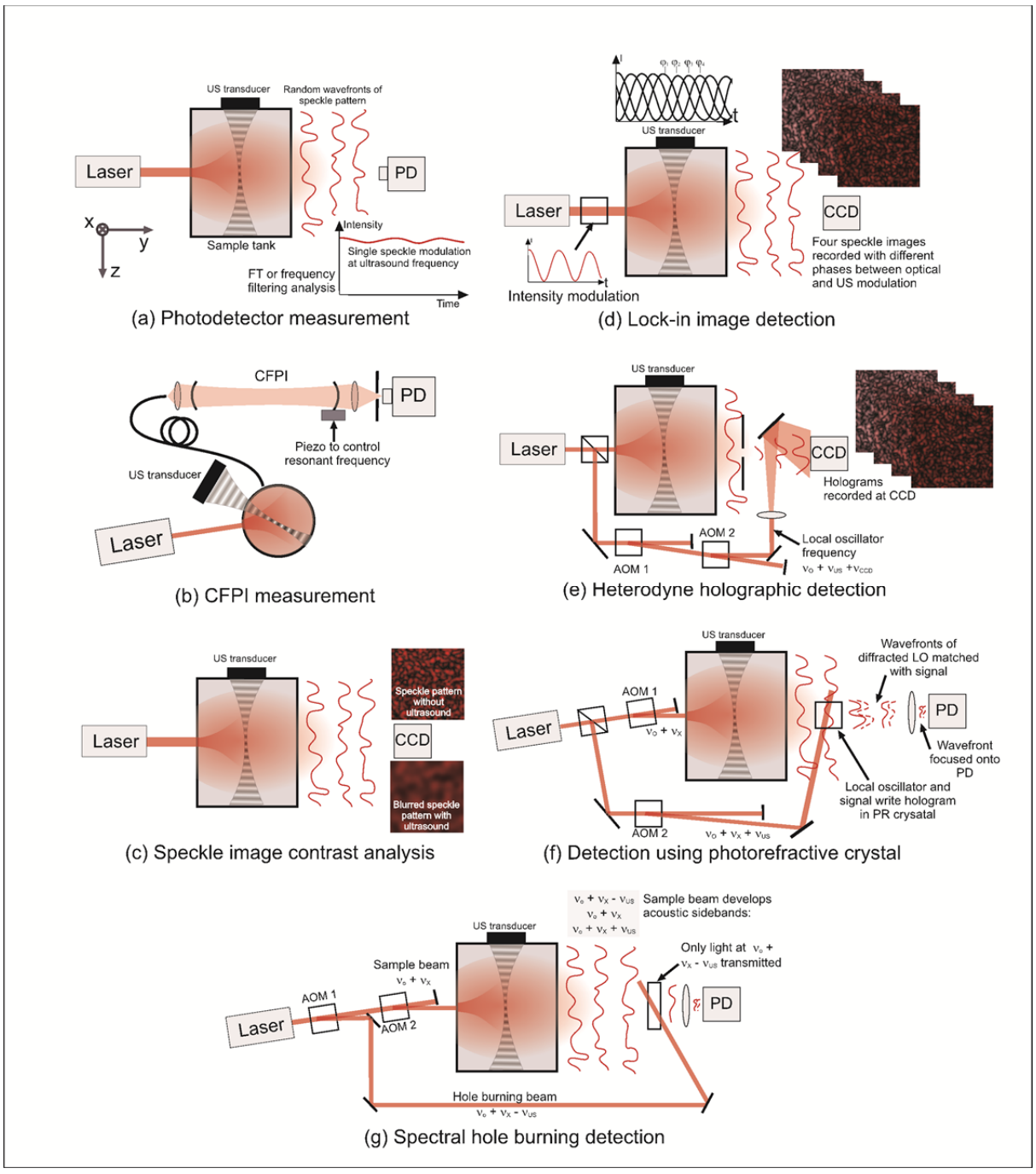

Figure 3: Summary of the main methods used to detect UOT signals. (a) Photodetector measurement, (b) confocal Fabry-Perot interferometer detection, (c) speckle image contrast analysis, (d) lock-in image detection, (e) heterodyne holographic detection, (f) detection using a photorefractive crystal, (g) spectral hole burning detection. PD – photodetector, AOM – acousto-optic modulator, PR – photorefractive crystal, ν_O - optical frequency, ν_{US} - ultrasound frequency, ν_X – frequency shift (typically ~ 70-80 MHz), ν_{CCD} – CCD camera frequency.

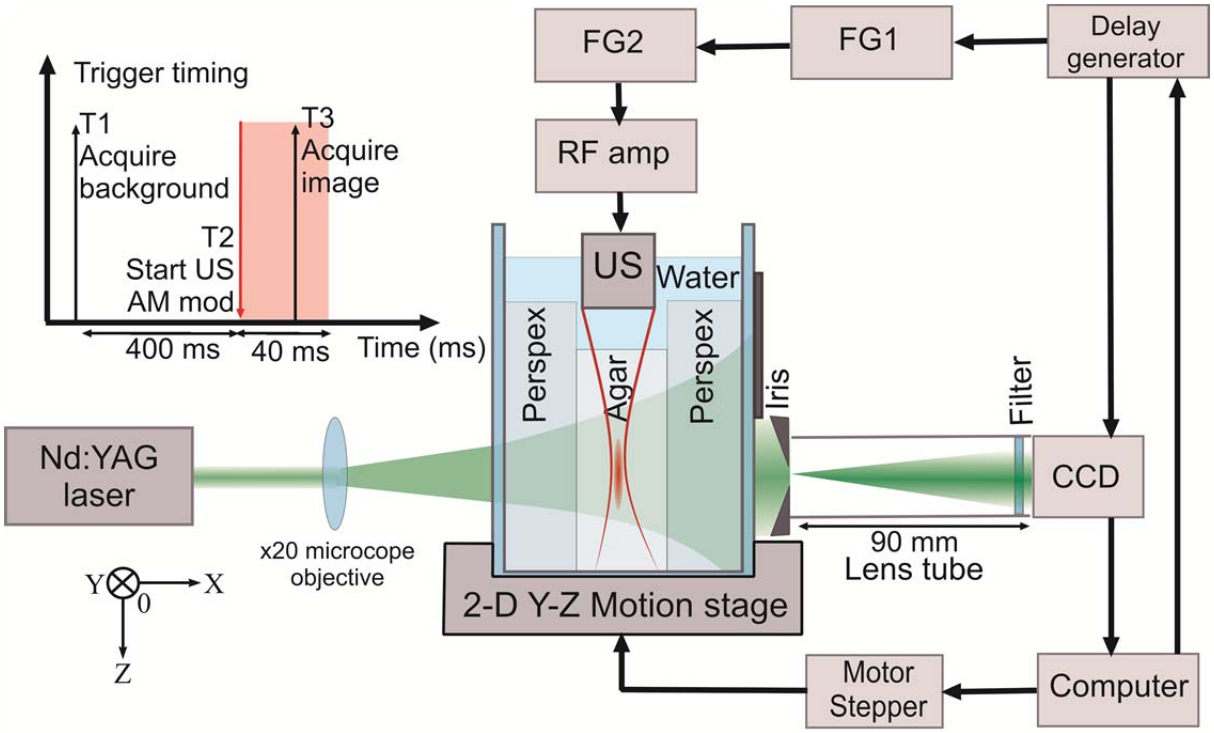

Figure 4: Experimental set-up. FG – frequency generator, US – ultrasound transducer. The trigger timing controlled by a Stanford DG535 is also illustrated showing: T1 - triggering the CCD camera when the ultrasound is off, T2 - triggering the function generators to produce the ultrasound signal, T3 - triggering the CCD camera when the ultrasound is on. The UOT signal is found from the difference in contrast between the two CCD exposures.

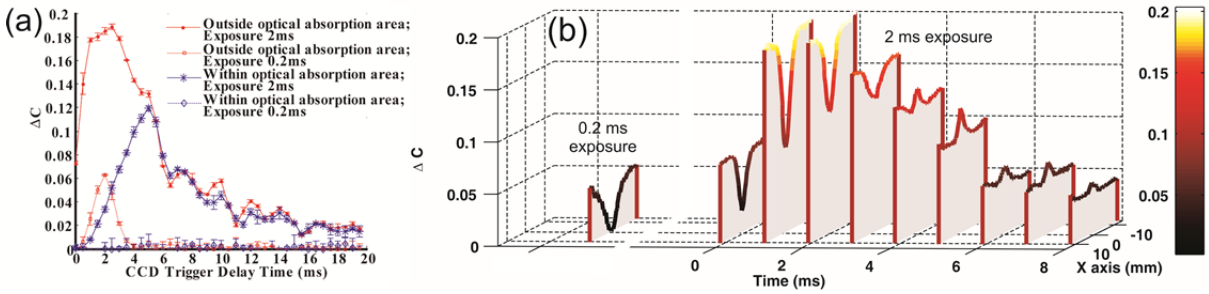

Figure 5(a) Contrast difference versus CCD trigger delay time for a 250 Hz-AM ultrasound burst with 0.2 ms and 2 ms CCD exposure time in a homogeneous area (blue line) and an absorbing area (red line) (b) Comparison between a 1-D profile of an optical absorber obtained with a 0.2 ms CCD exposure time measured 2 ms after launching a 250 Hz-AM acoustic burst (red line) and 1-D profiles with a 2 ms CCD exposure time measured at varying delay times after launching a 250 Hz-AM acoustic burst (Reproduction permission to be obtained from [103]).

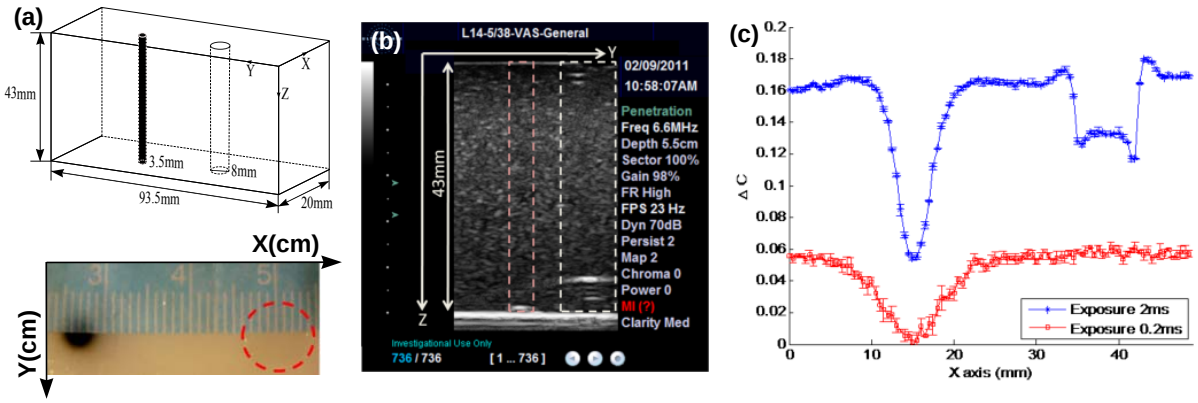

Figure 6: (a) Illustration of the phantom and a photograph of the cross-section taken after the experiments. The diameter of the Indian ink optical inclusion (on the left) was ~3.5 mm. The diameter of the stiffer inclusion (on the right inside the red-dashed circle) was ~8 mm. (b) B-mode ultrasound image of the phantom in the Y-Z plane showing no contrast from the optical or mechanical inclusions. (c) 1-D profiles of the inhomogeneous phantom measured with various CCD exposure times and CCD delay times. Again the optical inclusion was on the left and the stiffer inclusion was on the right. (Reproduction permission to be obtained from [103])

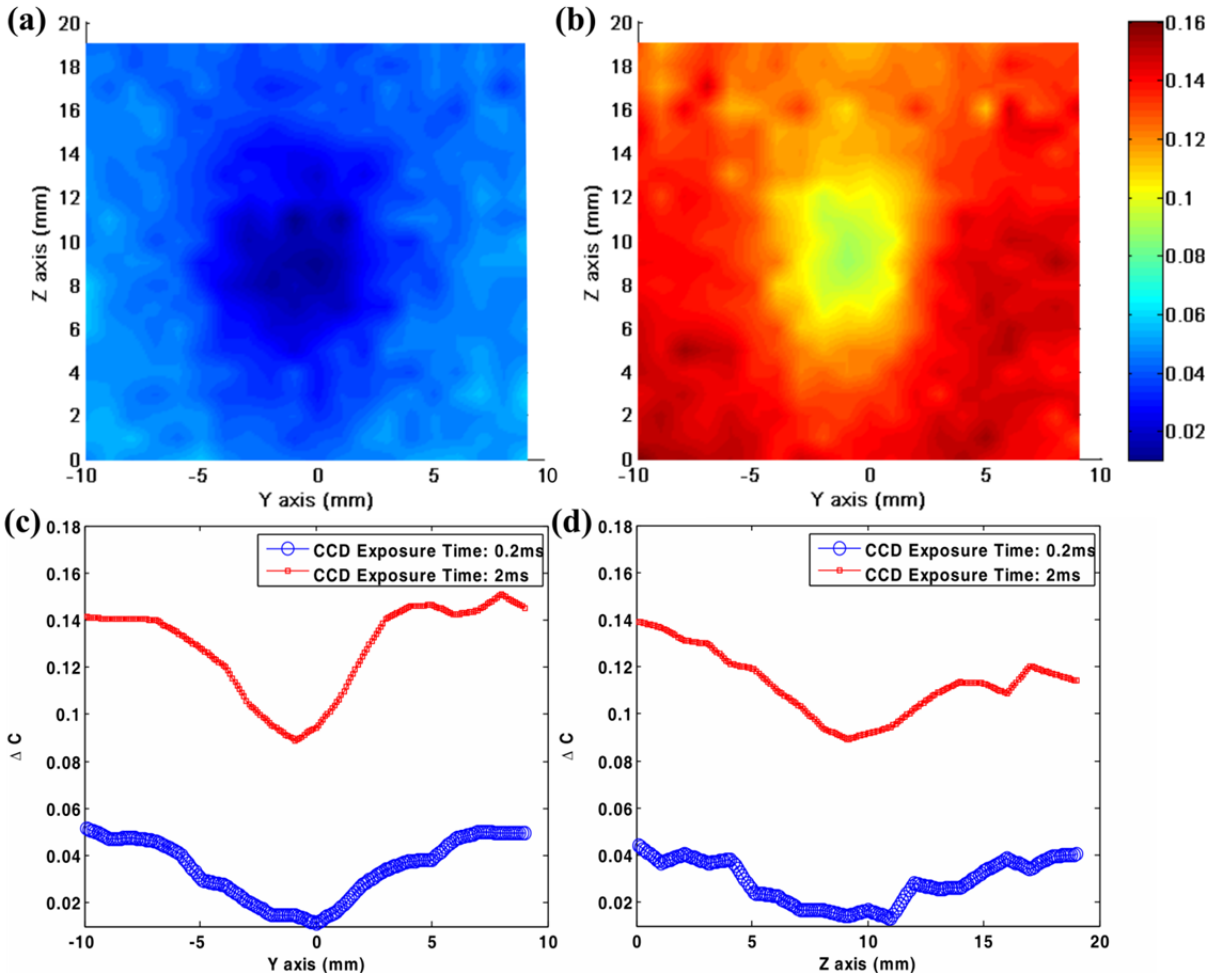

Figure 7: (a) A 2-D profile of an inhomogeneous phantom measured with a 0.2 ms CCD exposure time and a 2 ms CCD trigger delay time. (b) A 2-D profile of an inhomogeneous phantom measured with a 2 ms CCD exposure time and a 1ms CCD trigger delay time. (c) 1-D profiles taking along the midline (Z = 9 mm) from (a) and (b). (d) 1-D profiles taking along the midline (Y = 0 mm) from (a) and (b).

References

1 American National Standards Institute or International Commission on Non-Ionizing Radiation Protection

2 Linder, T. E., Simmen, D. & Stool, S. E. 1997 Revolutionary inventions in the 20th century - The history of endoscopy. *Archives of Otolaryngology-Head & Neck Surgery* **123**, 1161-1163.

3 Gono, K., Yamazaki, K., Doguchi, N., Nonami, T., Obi, T., Yamaguchi, M., Ohyama, N., Machida, H., Sano, Y., Yoshida, S., Hamamoto, Y. & Endo, T. 2003 Endoscopic observation of tissue by narrowband illumination. *Optical Review* **10**, 211-215.

4 Jocham, D., Witjes, F., Wagner, S., Zeylemaker, B., van Moorselaar, J., Grimm, M. O., Muschter, R., Popken, G., Konig, F., Knuchel, R. & Kurth, K. H. 2005 Improved detection and treatment of bladder cancer using hexaminolevulinate imaging: A prospective, phase III multicenter study. *Journal of Urology* **174**, 862-866.

5 Meining, A. & Wallace, M. B. 2008 Endoscopic imaging of angiogenesis in vivo. *Gastroenterology* **134**, 915-918.

6 Polglase, A. L., McLaren, W. J., Skinner, S. A., Kiesslich, R., Neurath, M. F. & Delaney, P. M. 2005 A fluorescence confocal endomicroscope for in vivo microscopy of the upper- and the lower-GI tract. *Gastrointestinal Endoscopy* **62**, 686-695.

7 Fu, L., Jain, A., Xie, H. K., Cranfield, C. & Gu, M. 2006 Nonlinear optical endoscopy based on a double-clad photonic crystal fiber and a MEMS mirror. *Optics Express* **14**, 1027-1032.

8 Fujimoto, J. G. 2003 Optical coherence tomography for ultrahigh resolution in vivo imaging. *Nature Biotechnology* **21**, 1361-1367.

9 Vo-Dinh, T. 2003 *Biomedical Photonics Handbook, Chapter 2*. New York: CRC.

10 Gibson, A. P., Hebden, J. C. & Arridge, S. R. 2005 Recent advances in diffuse optical imaging. *Physics in Medicine and Biology* **50**, R1-R43.

11 Arridge, S. R. 1999 Optical tomography in medical imaging. *Inverse Problems* **15**, R41-R93.

12 Leveque, S., Boccara, A. C., Lebec, M. & Saint-Jalmes, H. 1999 Ultrasonic tagging of photon paths in scattering media: parallel speckle modulation processing. *Optics Letters* **24**, 181-183.

13 Lai, P. X., Roy, R. A. & Murray, T. W. 2009 Quantitative characterization of turbid media using pressure contrast acousto-optic imaging. *Optics Letters* **34**, 2850-2852.

14 Marks, F. A., Tomlinson, H. W. & Brooksby, G. W. 1993 A comprehensive approach to breast-cancer detection using light - photon localization by ultrasound modulation and tissue characterization spectral discrimination. *Proceedings of Photon Migration and Imaging in Random Media and Tissues* **1888**, 500-510.

15 Lev, A., Kotler, Z., Sfez, B., Soustiel, J. & Feinsod, M. 2002 Non invasive local cerebral oxygenation monitoring using a combination of light and ultrasound. *Intracranial Pressure and Brain Biochemical Monitoring* **81**, 295-297.

16 Li, J. & Wang, L. H. V. 2004 Ultrasound-modulated optical computed tomography of biological tissues. *Applied Physics Letters* **84**, 1597-1599.

17 Lev, A., Rubanov, E., Sfez, B., Shany, S. & Foldes, A. J. 2005 Ultrasound-modulated light tomography assessment of osteoporosis. *Optics Letters* **30**, 1692-1694.

18 Kim, C., Song, K. H. & Wang, L. V. 2008 Sentinel lymph node detection ex vivo using ultrasound-modulated optical tomography. *Journal of Biomedical Optics* **13** Article No.: 020507.

19 Lai, P. X., McLaughlan, J. R., Draudt, A. B., Murray, T. W., Cleveland, R. O. & Roy, R. A. Real-time monitoring of high-intensity focused ultrasound lesion formation using acousto-optic sensing. *Ultrasound in Medicine and Biology* **37**, 239-252.

20 Tang, M. X., Elson, D. S., Li, R., Dunsby, C. & Eckersley, R. J. 2010 Photoacoustics, thermoacoustics, and acousto-optics for biomedical imaging. *Proceedings of the Institution of Mechanical Engineers Part H-Journal of Engineering in Medicine* **224**, 291-306.

21 Wang, L. H. V. 1998 Ultrasonic modulation of scattered light in turbid media and a potential novel tomography in biomedicine. *Photochemistry and Photobiology* **67**, 41-49.

22 Wang, L. H. V. 2003 Ultrasound-mediated biophotonic imaging: A review of acousto-optical tomography and photo-acoustic tomography. *Disease Markers* **19**, 123-138.

23 DiMarzio, C. A. & Murray, T. W. 2003 Medical imaging techniques combining light and ultrasound. *Subsurface Sensing Technologies and Applications* **4**, 289-309.

24 Goodman, J. W. 2007 *Speckle Phenomena in Optics: Theory and Applications*. Englewood, Colorado: Roberts & Company.

25 Kothapalli, S. R., Sakadzic, S., Kim, C. & Wang, L. V. 2007 Imaging optically scattering objects with ultrasound-modulated optical tomography. *Optics Letters* **32**, 2351-2353.

26 Xu, M. H. & Wang, L. H. V. 2006 Photoacoustic imaging in biomedicine. *Review of Scientific Instruments* 77 Article No.: 041101.

27 Wang, L. V. 2008 Prospects of photoacoustic tomography. *Medical Physics* **35**, 5758-5767.

28 Leutz, W. & Maret, G. 1995 Ultrasonic modulation of multiply scattered-light. *Physica B* **204**, 14-19.

29 Kempe, M., Larionov, M., Zaslavsky, D. & Genack, A. Z. 1997 Acousto-optic tomography with multiply scattered light. *Journal of the Optical Society of America A-Optics Image Science and Vision* **14**, 1151-1158.

30 Pine, D. J., Weitz, D. A., Chaikin, P. M. & Herbolzheimer, E. 1988 Diffusing-wave spectroscopy. *Physical Review Letters* **60**, 1134-1137.

31 Blonigen, F. J., Nieva, A., DiMarzio, C. A., Manneville, S., Sui, L., Maguluri, G., Murray, T. W. & Roy, R. A. 2005 Computations of the acoustically induced phase shifts of optical paths in acoustophotonic imaging with photorefractive-based detection. *Applied Optics* **44**, 3735-3746.

32 Born, M. & Wolf, E. 1999 *Principles of Optics*. Cambridge: Cambridge University Press.

33 Gross, M., Lesaffre, M., Ramaz, F., Delaye, P., Roosen, G. & Boccara, A. C. 2009 Detection of the tagged or untagged photons in acousto-optic imaging of thick highly scattering media by photorefractive adaptive holography. *European Physical Journal E* **28**, 173-182.

34 Wang, L. H. V. 2001 Mechanisms of ultrasonic modulation of multiply scattered coherent light: An analytic model. *Physical Review Letters* **87** Article No.: 043903.

35 Sakadzic, S. & Wang, L. V. 2005 Modulation of multiply scattered coherent light by ultrasonic pulses: An analytical model. *Physical Review E* **72** Article No.: 036620.

36 Sakadzic, S. & Wang, L. H. V. 2006 Correlation transfer and diffusion of ultrasound-modulated multiply scattered light. *Physical Review Letters* **96**.

37 Sakadzic, S. & Wang, L. V. 2007 Correlation transfer equation for multiply scattered light modulated by an ultrasonic pulse. *Journal of the Optical Society of America A-Optics Image Science and Vision* **24**, 2797-2806.

38 Blonigen, F. J., Nieva, A., DiMarzio, C. A., Manneville, S., Sui, L., Maguluri, G., Murray, T. W. & Roy, R. A. 2005 Computations of the acoustically induced phase shifts of optical paths in acoustophotonic imaging with photorefractive-based detection. *Applied Optics* **44**, 3735-3746.

39 Li, R., Song, L. P., Elson, D. S. & Tang, M. X. 2010 Parallel detection of amplitude-modulated, ultrasound-modulated optical signals. *Optics Letters* **35**, 2633-2635.

40 Wang, L. H. V. 2001 Mechanisms of ultrasonic modulation of multiply scattered coherent light: a Monte Carlo model. *Optics Letters* **26**, 1191-1193.

41 Leung, T. S. & Powell, S. 2010 Fast Monte Carlo simulations of ultrasound-modulated light using a graphics processing unit. *Journal of Biomedical Optics* **15** Article No.: 055007.

42 Elazar, J. M. & Steshenko, O. 2008 Doppler effect's contribution to ultrasonic modulation of multiply scattered coherent light: Monte Carlo modeling. *Optics Letters* **33**, 131-133.

43 Yao, G. & Wang, L. H. V. 2000 Theoretical and experimental studies of ultrasound-modulated optical tomography in biological tissue. *Applied Optics* **39**, 659-664.

44 Yao, G. & Wang, L. H. V. 2004 Signal and noise in ultrasound-modulated optical tomography: a Monte Carlo Study. *Photons Plus Ultrasound: Imaging and Sensing* **5320**, 156-163.

45 Lev, A. & Sfez, B. 2003 In vivo demonstration of the ultrasound-modulated light technique. *Journal of the Optical Society of America A-Optics Image Science and Vision* **20**, 2347-2354.

46 Gross, M., Goy, R., Forget, B. C., Atlan, M., Ramaz, E., Boccara, A. C. & Dunn, A. K. 2005 Heterodyne detection of multiply scattered monochromatic light with a multipixel detector. *Optics Letters* **30**, 1357-1359.

47 Wang, L. H., Jacques, S. L. & Zhao, X. M. 1995 Continuous-wave ultrasonic modulation of scattered laser-light to image objects in turbid media. *Optics Letters* **20**, 629-631.

48 Lev, A., Kotler, Z. & Sfez, B. G. 2000 Ultrasound tagged light imaging in turbid media in a reflectance geometry. *Optics Letters* **25**, 378-380.

49 Hisaka, M., Sugiura, T. & Kawata, S. 2001 Optical cross-sectional imaging with pulse ultrasound wave assistance. *Journal of the Optical Society of America A-Optics Image Science and Vision* **18**, 1531-1534.

50 Leveque-Fort, S., Selb, J., Pottier, L. & Boccara, A. C. 2001 In situ local tissue characterization and imaging by backscattering acousto-optic imaging. *Optics Communications* **196**, 127-131.

51 Li, J., Sakadzic, S., Ku, G. & Wang, L. H. V. 2003 Transmission- and side-detection configurations in ultrasound-modulated optical tomography of thick biological tissues. *Applied Optics* **42**, 4088-4094.

52 Granot, E., Lev, A., Kotler, Z., Sfez, B. G. & Taitelbaum, H. 2001 Detection of inhomogeneities with ultrasound tagging of light. *Journal of the Optical Society of America A-Optics Image Science and Vision* **18**, 1962-1967.

53 Wang, L. H., Jacques, S. L. & Zheng, L. Q. 1995 MCML - Monte-Carlo modeling of light transport in multilayered tissues. *Computer Methods and Programs in Biomedicine* **47**, 131-146.

54 Yao, G. & Wang, L. H. V. 2000 Theoretical and experimental studies of ultrasound-modulated optical tomography in biological tissue. *Applied Optics* **39**, 659-664.

55 Yao, Y., Xing, D., He, Y. H. & Ueda, K. 2001 Acousto-optic tomography using amplitude-modulated focused ultrasound and a near-IR laser. *Quantum Electronics* **31**, 1023-1026.

56 Rousseau, G., Blouin, A. & Monchalin, J. P. 2008 Ultrasound-modulated optical imaging using a powerful long pulse laser. *Optics Express* **16**, 12577-12590.

57 Kim, C. H. & Wang, L. V. 2007 Multi-optical-wavelength ultrasound-modulated optical tomography: a phantom study. *Optics Letters* **32**, 2285-2287.

58 Bratchenia, A., Molenaar, R., van Leeuwen, T. G. & Kooyman, R. P. H. 2009 Millimeter-resolution acousto-optic quantitative imaging in a tissue model system. *Journal of Biomedical Optics* **14** Article No.: 034031

59 Monchalin, J. P., Heon, R., Bouchard, P. & Padioleau, C. 1989 Broad-band optical-detection of ultrasound by optical sideband stripping with a confocal Fabry-Perot. *Applied Physics Letters* **55**, 1612-1614.

60 Sakadzic, S. & Wang, L. H. V. 2004 High-resolution ultrasound-modulated optical tomography in biological tissues. *Optics Letters* **29**, 2770-2772.

61 Wang, L. H. & Zhao, X. M. 1997 Ultrasound-modulated optical tomography of absorbing objects buried in dense tissue-simulating turbid media. *Applied Optics* **36**, 7277-7282.

62 Monchalin, J. P. 1985 Optical-detection of ultrasound at a distance using a confocal Fabry-Perot-interferometer. *Applied Physics Letters* **47**, 14-16.

63 Kothapalli, S.-R. & Wang, L. V. 2008 Ultrasound-modulated optical microscopy. *Journal of Biomedical Optics* **13**, Article No.: 054046.

64 Kothapalli, S. R. & Wang, L. H. V. 2009 Ex vivo blood vessel imaging using ultrasound-modulated optical microscopy. *Journal of Biomedical Optics* **14** Article No.: 014015.

65 Li, Y. Z., Hemmer, P., Kim, C. H., Zhang, H. L. & Wang, L. H. V. 2008 Detection of ultrasound-modulated diffuse photons using spectral-hole burning. *Optics Express* **16**, 14862-14874.

66 Gross, M., Goy, P. & Al-Koussa, M. 2003 Shot-noise detection of ultrasound-tagged photons in ultrasound-modulated optical imaging. *Optics Letters* **28**, 2482-2484.

67 Tomlinson, H. W. & Tiemann, J. J. 1993 Light imaging in a scattering medium, using ultrasonic probing and speckle image differencing (ed. U. P. Office). USA: General Electric Company.

68 Fercher, A. F. & Briers, J. D. 1981 Flow visualization by means of single-exposure speckle photography. *Optics Communications* **37**, 326-330.

69 Li, J., Ku, G. & Wang, L. H. V. 2002 Ultrasound-modulated optical tomography of biological tissue by use of contrast of laser speckles. *Applied Optics* **41**, 6030-6035.

70 Gleyzes, P., Guernet, F. & Boccara, A. C. 1995 Picometric profilometry . Multi detector approach and multiplexed lock-in detection. *Journal of Optics-Nouvelle Revue D Optique* **26**, 251-265.

71 Gross, M., Goy, P. & Al-Koussa, M. 2003 Shot-noise detection of ultrasound-tagged photons in ultrasound-modulated optical imaging. *Optics Letters* **28**, 2482-2484.

72 Le Clerc, F., Collot, L. & Gross, M. 2000 Numerical heterodyne holography with two-dimensional photodetector arrays. *Optics Letters* **25**, 716-718.

73 Yamaguchi, I. & Zhang, T. 1997 Phase-shifting digital holography. *Optics Letters* **22**, 1268-1270.

74 Blouin, A. & Monchalin, J. P. 1994 Detection of Ultrasonic Motion of a Scattering Surface by 2-Wave Mixing in a Photorefractive Gaas Crystal. *Applied Physics Letters* **65**, 932-934.

75 Murray, T. W., Sui, L., Maguluri, G., Roy, R. A., Nieva, A., Blonigen, F. & DiMarzio, C. A. 2004 Detection of ultrasound-modulated photons in diffuse media using the photorefractive effect. *Optics Letters* **29**, 2509-2511.

76 Ramaz, F., Forget, B. C., Atlan, M., Boccara, A. C., Gross, M., Delaye, P. & Roosen, G. 2004 Photorefractive detection of tagged photons in ultrasound modulated optical tomography of thick biological tissues. *Optics Express* **12**, 5469-5474.

77 Yariv, A. 1989 *Quantum Electronics*: Wiley.

78 Gross, M., Ramaz, F., Forget, B. C., Atlan, M., Boccara, C., Delaye, P. & Roosen, G. 2005 Theoretical description of the photorefractive detection of the ultrasound modulated photons in scattering media. *Optics Express* **13**, 7097-7112.

79 Gross, M., Lesaffre, M., Ramaz, F., Delaye, P., Roosen, G. & Boccara, A. C. 2009 Detection of the tagged or untagged photons in acousto-optic imaging of thick highly scattering media by photorefractive adaptive holography. *European Physical Journal E* **28**, 173-182.

80 Farahi, S., Montemezzani, G., Grabar, A. A., Huignard, J.-P. & Ramaz, F. 2010 Photorefractive acousto-optic imaging in thick scattering media at 790 nm with a $Sn_2P_2S_6$:Te crystal. *Optics Letters* **35**, 1798-1800.

81 Lesaffre, M., Jean, F., Ramaz, F., Boccara, A. C., Gross, M., Delaye, P. & Roosen, G. 2007 In situ monitoring of the photorefractive response time in a self-adaptive wavefront holography setup developed for acousto-optic imaging. *Optics Express* **15**, 1030-1042.

82 Li, Y. Z., Zhang, H. L., Kim, C. H., Wagner, K. H., Hemmer, P. & Wang, L. V. 2008 Pulsed ultrasound-modulated optical tomography using spectral-hole burning as a narrowband spectral filter. *Applied Physics Letters* **93** Article No.: 011111.

83 Daoudi, K., Boccara, A. C. & Bossy, E. 2009 Detection and discrimination of optical absorption and shear stiffness at depth in tissue-mimicking phantoms by transient optoelastography. *Applied Physics Letters* **94** Article No.: 154103.

84 Lev, A. & Sfez, B. 2003 In vivo demonstration of the ultrasound-modulated light technique. *Journal of the Optical Society of America A-Optics Image Science and Vision* **20**, 2347-2354.

85 Selb, J., Pottier, L. & Boccara, A. C. 2002 Nonlinear effects in acousto-optic imaging. *Optics Letters* **27**, 918-920.

86 Yao, G., Jiao, S. L. & Wang, L. V. 2000 Frequency-swept ultrasound-modulated optical tomography in biological tissue by use of parallel detection. *Optics Letters* **25**, 734-736.

87 Forget, B. C., Ramez, F., Atlan, M., Selb, J. & Boccara, A. C. 2003 High-contrast fast Fourier transform acousto-optical tomography of phantom tissues with a frequency-chirp modulation of the ultrasound. *Applied Optics* **42**, 1379-1383.

88 Lesaffre, M. Farahi, S., Gross, M., Delaya, P., Boccara, A. C. & Ramaz, F. 2009 Acousto-optical coherence tomography using random phase jumps on ultrasound and light. *Optics Express* **17** 18211-18218.

89 Atlan, M., Forget, B. C., Ramaz, F., Boccara, A. C. & Gross, M. 2005 Pulsed acousto-optic imaging in dynamic scattering media with heterodyne parallel speckle detection. *Optics Letters* **30**, 1360-1362.

90 Bossy, E., Sui, L., Murray, T. W. & Roy, R. A. 2005 Fusion of conventional ultrasound imaging and acousto-optic sensing by use of a standard pulsed-ultrasound scanner. *Optics Letters* **30**, 744-746.

91 Sarvazyan, A. P., Rudenko, O. V., Swanson, S. D., Fowlkes, J. B. & Emelianov, S. Y. 1998 Shear wave elasticity imaging: A new ultrasonic technology of medical diagnostics. *Ultrasound in Medicine and Biology* **24**, 1419-1435.

92 Bercoff, J., Tanter, M., Muller, M. & Fink, M. 2004 The role of viscosity in the impulse diffraction field of elastic waves induced by the acoustic radiation force. *IEEE Transactions on Ultrasonics Ferroelectrics and Frequency Control* **51**, 1523-1536.

93 Torr, G. R. 1984 The acoustic radiation force. *American Journal of Physics* **52**, 402-408.

94 Altberg, W. 1903 Über die Druckkräfte der Schallwellen und die absolute Messung der Schallintensitä. *Annalen der Physik* **316**, 405-420.

95 Nightingale, K., Soo, M. S., Nightingale, R. & Trahey, G. 2002 Acoustic radiation force impulse imaging: In vivo demonstration of clinical feasibility. *Ultrasound in Medicine and Biology* **28**, 227-235.

96 Fatemi, M. & Greenleaf, J. F. 1998 Ultrasound-stimulated vibro-acoustic spectrography. *Science* **280**, 82-85.

97 Athanasiou, A., Tardivon, A., Tanter, M., Sigal-Zafrani, B., Bercoff, J., Eux, T. D., Gennisson, J. L., Fink, M. & Neuenschwander, S. 2010 Breast lesions: quantitative elastography with supersonic shear imaging-preliminary results. *Radiology* **256**, 297-303.

98 Lev, A. & Sfez, B. G. 2003 Pulsed ultrasound-modulated light tomography. *Optics Letters* **28**, 1549-1551.

99 Kim, C., Zemp, R. J. & Wang, L. H. V. 2006 Intense acoustic bursts as a signal-enhancement mechanism in ultrasound-modulated optical tomography. *Optics Letters* **31**, 2423-2425.

100 Zemp, R. J., Kim, C. & Wang, L. V. 2007 Ultrasound-modulated optical tomography with intense acoustic bursts. *Applied Optics* **46**, 1615-1623.

101 Singh, M. S., Yalavarthy, P. K., Vasu, R. M. & Rajan, K. 2010 Assessment of ultrasound modulation of near infrared light on the quantification of scattering coefficient. *Medical Physics* **37**, 3744-3751.

102 Bossy, E., Funke, A. R., Daoudi, K., Boccara, A. C., Tanter, M. & Fink, M. 2007 Transient optoelastography in optically diffusive media. *Applied Physics Letters* **90** Article No.: 174111.

103 Li, R., Elson, D. S., Dunsby, C., Eckersley, R. & Tang, M. X. 2011 Effects of acoustic radiation force and shear waves for absorption and stiffness sensing in ultrasound modulated optical tomography. *Optics Express* **19** 7299-7311.